GJR Publication
OPEN ACCESS

Global Journal of Research in Engineering & Computer Sciences
ISSN: 2583-2727 (Online)
Volume 04| Issue 01 | Jan.-Feb. | 2024
Journal homepage: https://gjrpublication.com/gjrecs/

Review Article

# Application of Reduced-order Suboptimal H_∞ Control for Vertical Oscillation Damping in Mass-spring-dashpot Systems

Muhammad Auwal Shehu[1], *Muhammad Baballe Ahmad[2], Aminu Abdullahi Umar[3], Aliyu Surajo[4], Haruna Garba Rabo[5]

[1, 2, 3, 4,5] Department of Mechatronic Engineering, Nigerian Defence Academy (NDA), Kaduna, Nigeria

**DOI:** 10.5281/zenodo.10651888 **Submission Date:** 22 Dec. 2024 | **Published Date:** 13 Feb. 2024

***Corresponding author:** **Muhammad Baballe Ahmad**
Department of Mechatronic Engineering, Nigerian Defence Academy (NDA), Kaduna, Nigeria
**ORCID:** 0000-0001-9441-7023

## Abstract

This paper focuses on the robust stability and performance of suboptimal $\mathcal{H}_\infty$ control on mass-spring-dashpot systems subject to parametric uncertainty and external disturbances. The objective is keeping the vertical displacement of the system constant under uncertainty and disturbance. For the control system to achieve satisfactory performance, suitable weighting filter functions for performance and control effort were respectively designed. Model order reduction for the synthesized controller based on Hankel norm approximation was conducted, where a third order controller was obtained. Numerical results based on µ-analysis, frequency response and transient response showed that the closed-system achieved satisfactory robustness in the presence of parametric uncertainty and disturbance over the entire frequency bandwidth of study.

**Keywords:** $\mathcal{H}_\infty$ control, Linear fractional transform, Structured uncertainties, Frequency analysis, µ-analysis.

## INTRODUCTION

Disturbances such as sensor measurement noise, actuator noise, and parameter uncertainties affect the performance of dynamical systems [1]. Also, modelling errors such as un-modelled dynamics, model-order-reduction, linearization also affect control effectiveness. Not to mention, it might be the case where the structure of the model is known but the system is (parametrically) uncertain. These discrepancies between the actual system and its mathematical representation are inexorable. Thus, in control design, a single transfer function cannot be used to precisely describe the practical system. One solution is to come up with sets of models that contain the actual system under study and then quantify the uncertainty bound between the actual system and its model.

The disturbance and model uncertainty are the driving factors for using feedback [2],[3]. Hence, modelling disturbance and uncertainty is crucial in control design. One approach that can be utilized for disturbance and uncertainty modelling is to describe the actual plant by a nominal plant and some characterization of the uncertainty [2]. Due to shortcomings of a model to precisely emulate the practical system, robustness has become a crucial factor in design of control systems [4]. Robust control is particularly concerned with powerful methods for the analysis and design of control systems in the presence of uncertainties [5]. In robust control, there are two kinds of specifications: *robust stability* and *robust performance*. To avoid difficulty in control system design, it is crucial to convert the two different specifications into the same type, mathematically. Favourably, when performance specification is in terms of $\mathcal{H}_\infty$ norm, it is synonymous to a certain robust stability problem [1].

An analytical plant model for use in the derivation of linearized uncertainty model for control design is needed. It allows us to easily obtain both parametric and unstructured uncertainty models [3]. Some methodologies were proposed for the design of compensators for some sort of *mass-spring-dashpot systems* (MSD) [6]-[11]. In [6] robust µ-synthesis for MSD with spring stiffness constant uncertainty was studied. For each level of uncertainty, a compensator was designed to maximize the performance. Like in [6], the spring stiffness constant uncertainty was studied in [7] but using the $\mathcal{H}_\infty$ loop-shaping control. Other robust control methods proposed in the literature for the control of the MSD include

the $\mathcal{H}_\infty$ with mixed sensitivity in [8], robust control system design using random search and genetic algorithms in [9], to mention but only a few.

In this work, the dynamics of a single-stage MSD system with parametric uncertainties in mass, spring and dashpot under the influence of exogenous disturbance is studied. To achieve *robust stability* and *robust performance* over a bandwidth of 0.01-100 rad/sec in the presence of these uncertainties and exogenous disturbance, the robust (sub)optimal $\mathcal{H}_\infty$ control is designed. Suitable control and performance weighting filter functions have been designed. The rest of the paper is organized as follows. In second section, we present the mathematical modelling of the nominal plant followed by uncertainty modelling. Third section is devoted to the design of (sub)optimal $\mathcal{H}_\infty$ feedback controller. Discussion on formulation of the robust design problem into minimization problem is presented followed by filter functions design and controller order reduction. In section four, the frequency domain and time domain simulation results are discussed. Section five concludes the paper.

**System Description and Modelling**

As shown in Fig. 1a, the system under study is a single-stage, fixed-base configuration MSD with spring and dashpot in parallel. The system parameters and variables are described in Table I. Additionally, the free-body-diagram of the system is shown in Fig. 1b to deriving the equation-of-motion for the system. Based on Newton's second motion law, the *force of inertia* $F_m$ due to the mass $m$ is given by [12]:

$$F_m = m\frac{d^2q(t)}{dt^2} = m\ddot{q}(t) \tag{1}$$

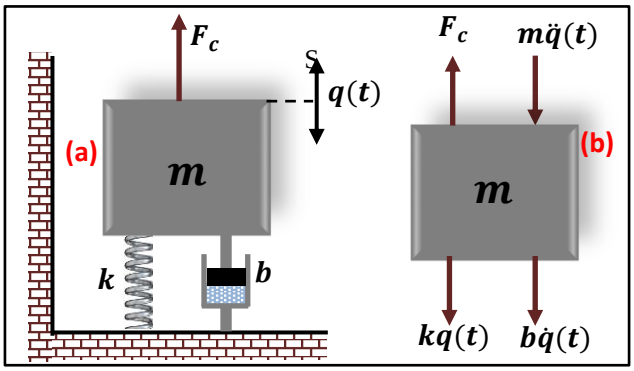


**Figure 1: Mass-spring-dashpot system; (a) system; (b) free-body-diagram**

Perturbing the system by an external force, the system is subjected to vibration which decreases gradually. Consequently, the displacement amplitude gradually decays. The mechanism by which the vibrational energy is gradually decays is called damping [13]. The *damping force* $f_b$ of the dashpot is [14]:

$$F_b = b\frac{dq(t)}{dt} = b\dot{q}(t) \tag{2}$$

And by Newton's motion law, the *spring force* $F_k$ due to the spring k is given by [15]:

$$F_k = kq(t) \tag{3}$$

With respect to Fig. 1b, the three forces in (1), (2) and (3) oppose the exogenous control force $F_c = u$. The net forces acting on the system gives the equation-of-motion for the system expressed as:

$$m\ddot{q}(t) + b\dot{q}(t) + kq(t) - F_c = 0 \tag{4}$$

The block diagram for the system in (4) is shown in Fig. 2. In practice, the precise values for the parameters $m$, $b$, and $k$ are not known. Even if known, the parameters are susceptible to alterations due to environmental changes and torn-and-worn factors. Anyhow, the values of the system parameters are assumed to be bounded, that is:

$$m = m_o(1 + p_m\Delta_m), b = b_o(1 + p_b\Delta_b), k = k_o(1 + p_k\Delta_k) \tag{5}$$

where $m_o$, $b_o$, and $k_o$ denote the nominal parameters of the system defined in Table I, $p_m$, $p_b$ and $p_k$ and $\Delta_m$, $\Delta_b$, and $\Delta_k$ represent possible perturbations on nominal values of the respective system parameters denoted by the subscripts. In this study, parametric variations of 30% above and below the nominal values are assumed, hence, $p_m = p_b = p_k = 0.3$ and $-1 \leq \Delta_m, \Delta_b, \Delta_k \leq 1$.

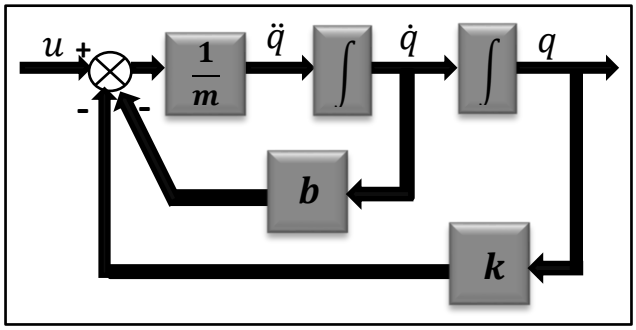


**Figure 2: Mass-spring-dashpot system block diagram**

**Table I: Simulation model parameters and description of variables**

| Notation | Description | Value | Unit |
|---|---|---|---|
| $m_o$ | Nominal mass | 3.5 | Kg |
| $b_o$ | Nominal viscous damping coefficient | 1.2 | N($ms^{-1}$) |
| $k_o$ | Nominal spring stiffness constant | 2.2 | N/m |
| $p_m$ | Possible relative perturbation on $m_o$ | 30 | % |
| $p_b$ | Possible relative perturbation on $b_o$ | 30 | % |
| $p_k$ | Possible relative perturbation on $k_o$ | 30 | % |
| q | Displacement | - | m |
| q̇ | Velocity | - | $ms^{-1}$ |
| q̈ | Acceleration | - | $ms^{-2}$ |
| $F_c$ | External control force | - | N |

From Fig. 2, the parameter block $1/m$ can be expressed in terms of the nominal value $m_o$ and perturbation variable $\Delta_m$. It follows that, representing $1/m$ in linear fractional transform (LFT) with respect to the uncertainty $\Delta_m$ and noting that (5) applies, it is easy to obtain (6). Following similar approach for parameter blocks $b$ and $k$ in terms of perturbation variables $\Delta_b$ and $\Delta_k$ we obtain (7) and (8) respectively.

$$\frac{1}{m} = \mathcal{F}_u(M_m, \Delta_m) \tag{6}$$

$$b = \mathcal{F}_u(M_c, \Delta_c) \tag{7}$$

$$k = \mathcal{F}_u(M_k, \Delta_k) \tag{8}$$

where

$$M_m = \begin{bmatrix} -p_m & 1/m_o \\ -p_m & 1/m_o \end{bmatrix}, M_b = \begin{bmatrix} 0 & b_o \\ p_b & b_o \end{bmatrix}, M_k = \begin{bmatrix} 0 & k_o \\ p_k & k_o \end{bmatrix}.$$

We can represent the system in LFT form of the perturbation variables. This is shown in Fig. 3 where the inputs and outputs to the perturbation blocks $\Delta_m, \Delta_b$ and $\Delta_k$ are denoted as $u_m, u_b, u_k$ and $y_m, y_b, y_k$ respectively. When the LFT form holds, it is easy to show that the input-output equations for the perturbed variables are:

$$\begin{cases} \begin{bmatrix} y_m \\ \ddot{x} \end{bmatrix} = \begin{bmatrix} -p_m & 1/m_o \\ -p_m & 1/m_o \end{bmatrix} \begin{bmatrix} u_m \\ u - v_b - v_k \end{bmatrix} \\ \begin{bmatrix} y_b \\ v_b \end{bmatrix} = \begin{bmatrix} 0 & b_o \\ p_b & b_o \end{bmatrix} \begin{bmatrix} u_b \\ \dot{x} \end{bmatrix} \\ \begin{bmatrix} y_k \\ v_k \end{bmatrix} = \begin{bmatrix} 0 & k_o \\ p_k & k_o \end{bmatrix} \begin{bmatrix} u_k \\ x \end{bmatrix} \\ u_m = \Delta_m y_m, \quad u_b = \Delta_b y_b, \quad u_k = \Delta_k y_k \end{cases} \tag{9}$$

By setting $x_1 = q$ and $x_2 = \dot{q} = \dot{x}_1$, so that $\dot{x}_2 = \ddot{q} = \ddot{x}_1$, and choosing $x_1 = y$, one obtains:

$$\begin{cases} \dot{x}_1 = x_2 \\ \dot{x}_2 = -p_m u_m + {}^1/_{m_o}\,(u - v_b - v_k) \\ y_m = -p_m u_m + {}^1/_{m_o}\,(u - v_b - v_k) \\ y_b = b_o x_2 \\ y_k = k_o x_1 \\ v_b = p_b u_b + b_o x_2 \\ v_k = p_k u_k + k_o x_1 \\ y = x_1 \\ u_m = \Delta_m y_m, \quad u_b = \Delta_b y_b, \quad u_k = \Delta_k y_k \end{cases} \tag{10}$$

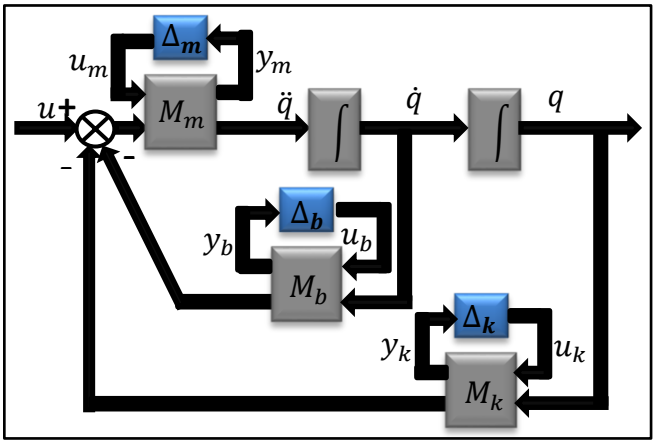


**Figure 3: System block diagram representation with uncertainties**

From (10), after a handful simplifications, the governing equations for the system in Fig. 3 are obtained as (11):

$$\begin{cases} \begin{bmatrix} \dot{x}_1 \\ \dot{x}_2 \\ \cdots \\ y_m \\ y_b \\ y_k \\ \cdots \\ y \end{bmatrix} = \begin{bmatrix} A & \vdots & B_1 & B_2 \\ \cdots\cdots & \cdots & \cdots & \cdots \\ C_1 & \vdots & D_{11} & D_{12} \\ C_2 & \vdots & D_{21} & 0 \end{bmatrix} \begin{bmatrix} x_1 \\ x_2 \\ \cdots \\ u_m \\ u_b \\ u_k \\ \cdots \\ u \end{bmatrix} \\ \begin{bmatrix} u_m \\ u_b \\ u_k \end{bmatrix} = diag(\Delta_m, \Delta_b, \Delta_k) \begin{bmatrix} y_m \\ y_b \\ y_k \end{bmatrix} \end{cases} \tag{11}$$

where

$$A = \begin{bmatrix} 0 & 1 \\ -\frac{k_o}{m_o} & -\frac{b_o}{m_o} \end{bmatrix}, B_1 = \begin{bmatrix} 0 & 0 & 0 \\ -p_m & -\frac{p_b}{m_o} & -\frac{p_k}{m_o} \end{bmatrix}, B_2 = \begin{bmatrix} 0 \\ \frac{1}{m_o} \end{bmatrix}, C_1 = \begin{bmatrix} -\frac{k_o}{m_o} & -\frac{b_o}{m_o} \\ 0 & b_o \\ k_o & 0 \end{bmatrix}, C_2 = [1 \quad 0]$$

$$D_{11} = \begin{bmatrix} -p_m & -\frac{p_b}{m_o} & -\frac{p_k}{m_o} \\ 0 & 0 & 0 \\ 0 & 0 & 0 \end{bmatrix}, D_{12} = \begin{bmatrix} \frac{1}{m_o} \\ 0 \\ 0 \end{bmatrix}, D_{21} = \begin{bmatrix} 0 \\ 0 \\ 0 \end{bmatrix}^T.$$

Based on the system dynamics in (11) which incorporates the parametric uncertainties, it can be seen that the system has two states $(x_1, x_2)$, four inputs $(u, u_m, u_b, u_k)$ and four outputs $(y, y_m, y_b, y_k)$. By denoting the input-output dynamics relations of the nominal system as $G_o$ the state-space equation for $G_o$ is:

$$G_o = \begin{bmatrix} A & \vdots & B_1 & B_2 \\ \cdots & \cdots & \cdots & \cdots \\ C_1 & \vdots & D_{11} & D_{12} \\ C_2 & \vdots & D_{21} & 0 \end{bmatrix} \tag{12}$$

The system can further be defined in upper LFT of the nominal plant with respect to the uncertainty Δ as:

$$y = x_1 = \mathcal{F}_U(G_o, \Delta)u \tag{13}$$

where $\Delta = diag(\Delta_m, \Delta_b, \Delta_k)$. $G_o$ is the nominal plant, while Δ is uncertainty matrix representing all probable uncertainties and is unknown but is assumed norm bounded ($\|\Delta\|_\infty < 1$).

## Control System Design

### A. *Suboptimal $\mathcal{H}_\infty$ Design*

At this point, the proposed control system is designed. A diagram of the control structure is shown in Fig. 4, where $G_o$ and Δ retain their definitions, $G_a$ denotes the uncertain plant, $e$ is the set-point tracking error and $F$ is feedback controller. Also, $\alpha_u$ and $\alpha_p$ are the control and performance weighting filter functions (to be designed) respectively, while $e_p$ and $e_u$ represent performance and control outputs in that order.

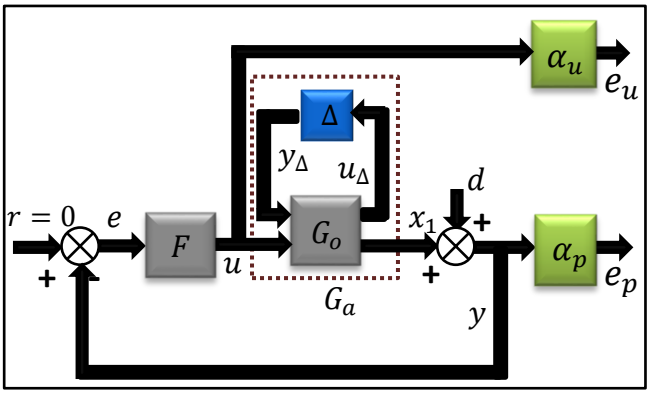


**Figure 4: Closed-loop system structure**

The control design problem is to find the optimal controller $F(s)$ for the linear output feedback control law $u(s) = F(s)y(s)$ that minimizes the cost function (14) over all sets of stabilizing controllers.

$$minimize \left\| \begin{bmatrix} S \\ FS \end{bmatrix} \right\|_\infty \tag{14}$$

Where

$$S := (I + G_oF)^{-1} = \frac{error\ (e)}{Setpoint(r) - disturbance(d)}$$

is known as the output sensitivity function of the plant $G_o$ and represents the transfer function of the set-point tracking error. The design goal in (14) is to minimize the sensitivity transfer function $S$ (which ensures good disturbance attenuation and tracking error) and the transfer function $FS$ (which takes care of robustness issue and keeping the control effort minimal). Generally, in order to meet design specifications, the cost function (14) is multiplied by the weighting functions $\alpha_u$ and $\alpha_p$. Consequently, with the weighting functions incorporated into the mixed-sensitivity (or *S/FS*) control design, we have the following minimization requirements:

- Nominal stability and performance requirement:

$$\left\| \begin{bmatrix} \alpha_p S \\ \alpha_u FS \end{bmatrix} \right\|_\infty < \gamma \tag{15}$$

- Robust stability and performance requirement:

$$\left\| \begin{bmatrix} \alpha_p (I + G_aF)^{-1} \\ \alpha_u F(I + G_aF)^{-1} \end{bmatrix} \right\|_\infty < \gamma \tag{16}$$

for a positive constant $\gamma < 1$. In (16) $(I + G_aF)^{-1}$ is the sentivity transfer function of the uncertain plant. It is also required to keep the order of the synthesized controller low.

In this study, all system parameters are assumed to vary from the nominal value by $\pm 30\%$ (i.e. $2.45 \ll m \leq 4.55, 0.84 \ll b \ll 1.56\ and\ 1.54 \ll k \leq 2.86$). If the closed-loop system remains *internally stable* in the presence of

these uncertainties, then the system is said to be *robustly stable* to all possible model variations. Equation (17) represents the performance criterion required to be minimal w.r.t $\|\cdot\|_\infty$ for all uncertainties.

$$\begin{bmatrix} e_p \\ e_u \end{bmatrix} = \begin{bmatrix} \alpha_p (I + G_a F)^{-1} \\ \alpha_u K (I + G_a F)^{-1} \end{bmatrix} d \tag{17}$$

## B. Selection of Weighting Functions

Disturbance is mostly having its power localized at low frequencies. Thus, it will be successfully rejected if the maximum singular value of the sensitivity function $S$ is made small over the same low frequencies. Assuming that the singular value of $(I + G_a F)^{-1}$ is known, we can set the singular value of $1/\alpha_p(s)$ greater than that of $(I + G_a F)^{-1}$ over all frequencies for "$\left\|\alpha_p(s)(I + G_a F)^{-1}\right\|_\infty < 1$" to hold. For "$\left\|\alpha_p(s)(I + G_a F)^{-1}\right\|_\infty < 1$" to hold, we must ensure that the singular values of the sensitivity function lie below those of $1/\alpha(s)_p$. As a deduction, a *low-pass filter* transfer function is selected as the performance weighting function $\alpha_p(S)$ to suppress the effect of the disturbance. The performance weighting filter transfer function can be obtained using [16]

$$\alpha_p(S) = \beta \frac{(\rho S^2 + 2\zeta_1 \omega_c \sqrt{\rho} S + \omega_c^2)}{(\beta S^2 + 2\zeta_2 \omega_c \sqrt{\beta} S + \omega_c^2)} \tag{18}$$

where $\rho$ represents the high frequency gain which deals with the system response overshoot, $\beta$ is disturbance rejection function *dc gain*, $\omega_c$ is *crossover frequency*, while $\xi_1$ and $\xi_2$ represents the *damping constants* of *crossover frequency*. Specified transient response requirements are assumed to be a settling time of less than 10s and a maximum overshoot of 25% for *robust stability* and *robust performance*.

In practice, "trial-and-check" method is usually employed to arrive at "best" weighting filter functions that meet design requirements. The performance weighting function is selected as (19) and the singular values response plot of the inverse of the performance weighting function is shown in Fig. 5a.

$$\alpha_p(S) = 0.1 \frac{S^2 + 4S + 100}{S^2 + 15S + 0.01} \tag{19}$$

Practically, the mass actuator has finite power and limited bandwidth of operation [16]. By making the control weights low at low frequencies and increased weights at higher frequencies, we can have a control system that can allow high values of control force at low frequencies, but small force amplitude at high frequencies. The control weighting function $\alpha_u(s)$ is required for reducing the high frequency part of the control input before it is sent to the actuator. A *high-pass filter* is usually selected for weighting the control input and to ensure robustness against uncertainties in the plant in the high frequency range [5],[6],[18]. For a good design, selecting a suitable weighting function is crucial. According to [16] the control weighting function can be obtained using:

$$\alpha_u(S) = \frac{S^2 + 2\frac{\omega_{bc}}{\sqrt{M_{FS}}} S + \frac{\omega_{bc}^2}{M_{FS}}}{\tau S^2 + 2\sqrt{\tau \omega_{bc}} S + \omega_{bc}^2} \tag{20}$$

where $M_{FS}$ is magnitude of $F(I + G_a F)^{-1}$, $\omega_{bc}$ is *control bandwidth* and $\tau$ is a small constant. Similarly, by "trial-and-check" tuning of control weighting function the weighting function is selected as (21). The corresponding singular values response plot of the inverse of the control weighting function is shown in Fig. 5b.

$$\alpha_u(S) = 10^2 \frac{S + 1 \times 10^{-1}}{S + 1 \times 10^6} \tag{21}$$

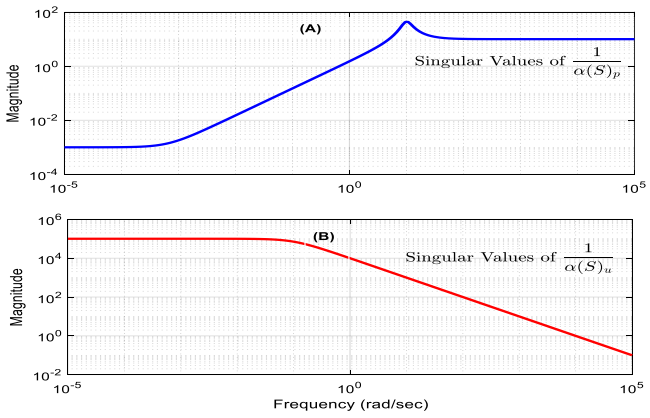


**Figure 5: Singular values for: (A) $\alpha_p(S)$ and (B) $\alpha_u(S)$**

From Fig. 5a, it is evident that using the designed performance weighting function (19), the closed-loop system would suppress the amplitudes of the output disturbance at low frequencies (up to about 9 rad/sec) in the ratio 1 to 0.001. Hence, the effect of a unit disturbance on the output or set-point tracking error at steady-state would be in the order of $\leq 10^{-3}$. It may have also been observed that, frequencies in excess of about 9 rad/sec are un-attenuated. Fortunately, the disturbance signal dwells at frequencies well below 9 rad/sec.

## C. *Controller Synthesis Methodology*

The MATLAB® *Robust Control Toolbox* (MRCT) can be used to carryout $\gamma$-iterations. MRCT command hinfsyn was used to synthesis the (sub)optimal $\mathcal{H}_\infty$ controller based on the open-loop interconnection system. The designed controller is to minimize $\|\mathcal{F}_L(G_o, F)\|_\infty$ over sets of stabilizing controllers. $\mathcal{F}_L(G_o, F)$ is the lower LFT of the nominal plant and the designed controller. Iterations were performed based on the bisection method with an *initial lower bound* $\gamma$-value of 0.1 and an *initial upper bound* $\gamma$-value of 1. *Relative error tolerance* for $\gamma$ is selected as $10^{-3}$. Iterations are performed on the initial bounds of $\gamma$ in an effort to approach the optimal full information $\mathcal{H}_\infty$ control design. A final $\gamma$-value of 0.1448 was achieved and a 5th order controller is obtained. The states-space matrices for the synthesized controller are obtained as (22):

$$\begin{cases} A_F = \begin{bmatrix} \frac{-345}{1006} & \frac{-1361}{1833} & \frac{677}{1575} & \frac{414}{4037} & \frac{12692}{381} \\ 1 & 0 & 0 & 0 & 0 \\ 0 & 0 & \frac{-25}{37516} & \frac{-41}{18893} & 0 \\ 0 & 0 & \frac{41}{18893} & \frac{-22514}{1501} & 0 \\ \frac{-5477}{19} & \frac{-5499}{24} & \frac{51581}{4} & \frac{73837}{24} & \frac{-38429}{61} \end{bmatrix} \\ B_F = \begin{bmatrix} 0 \\ 0 \\ \frac{5249}{643} \\ \frac{-5077}{382} \\ 0 \end{bmatrix}, \quad C_F = \begin{bmatrix} \frac{-95}{32956} & \frac{-139}{6110} & \frac{677}{5250} & \frac{125}{4063} & \frac{6346}{635} \end{bmatrix}, \quad D_F = 0 \end{cases} \tag{22}$$

## D. *Controller Order Reduction*

To this point, we have successfully obtained our synthesized $\mathcal{H}_\infty$ controller for the benchmark system under study. As mentioned earlier a 5th order controller is obtained (22). However, in practice the controller with the lowest order capable of satisfying control requirement, is preferred by practicing control engineers. Compared to lower order controllers, higher order controllers are relatively difficult and expensive to implement due to hardware limitations. The idea behind order reduction is to discard states, which are "weakly" *controllable* and *observable*. However, a mode may be weakly observable and highly controllable, or *vice versa*. In such a scenario, deleting such a *mode* may be inappropriate to the system dynamics. One way to deal with this is to obtain a *balanced realization* to obtain a "balance" for the *observability* and *controllability* of the system before it is reduced. Order reduction can be done using techniques such as *balanced truncation*, *balanced residualization*, *optimal Hankel-norm*, $\mathcal{H}_2$*-norm*, $\mathcal{H}_\infty$*-norm*, or *Markov and covariance parameter matching* techniques to mention but few. For brevity we are not discussing on these reduction techniques. Interested reader may refer to [21] for detailed treatment of these reduction techniques.

We employed the *optimal Hankel norm* method due to its accuracy at higher frequencies. The MRCT is utilized for reduction based using *optimal Hankel norm* approximation technique. The steps required are as follows:

1. Obtain a truncated *balanced realization* of the full-order system. This may be obtained using the MRCT command sysbal. All Hankel singular values (SVs) greater than defined tolerance tol are retained.
2. Next, compute the energy levels for the states of the balanced realized full-order controller model, for contribution evaluation. The MRCT command hsv may be used. At this stage table II is obtained.
3. Obtain the approximate controller.

Based on Table II, a 3rd order controller is selected and its state-space equation matrices are given as (23).

$$\begin{cases} A_{FR} = \begin{bmatrix} \frac{-7256}{721} & \frac{1106}{215} & \frac{-191}{1575} \\ \frac{-1487}{103} & \frac{-838}{387} & \frac{-62}{5075} \\ 0 & 0 & \frac{-192}{288191} \end{bmatrix} \\ B_{FR} = \begin{bmatrix} \frac{4232}{135} \\ \frac{2850}{179} \\ \frac{464}{153} \end{bmatrix} \quad C_{FR} = \begin{bmatrix} \frac{8821}{272} & \frac{2567}{189} & \frac{665}{219} \end{bmatrix} \quad D_{FR} = \begin{bmatrix} \frac{-1233}{409} \end{bmatrix} \end{cases} \tag{23}$$

In Fig. 6 the performances of full-order and reduced order controllers are compared based on frequency response. It may have been observed that the reduced order controller response matches that of the full order controller with respect to both magnitude and phase up to a frequency of about 120 rads/sec.

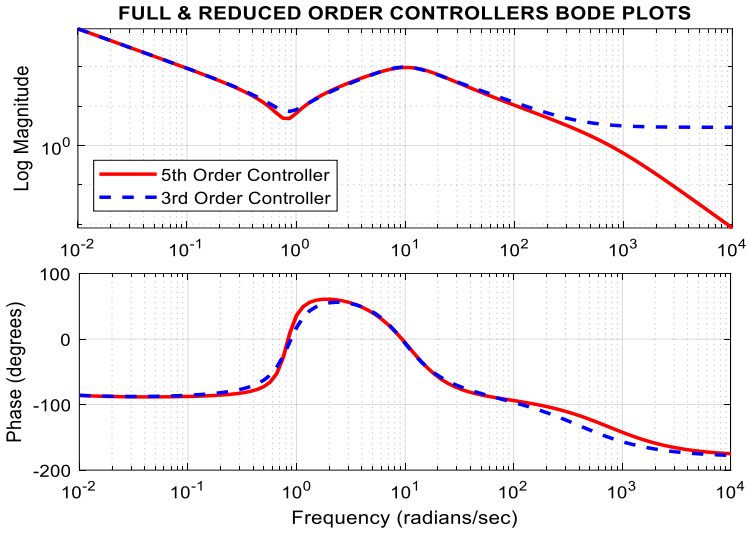


**Figure 6: Frequency response comparison for full-order and reduced-order controllers**

**Table II: Full order controller states contribution based on Hankel SVs**

| **State:** | 1 | 2 | 3 | 4 | 5 |
|---|---|---|---|---|---|
| **Hankel SVs:** | 6902.5 | 50.6 | 45.9 | 2.4 | 0.7 |

## Results and Performance Evaluations

The final $\gamma$-value of 0.1448 indicates that the condition "$\left\|\alpha_p(s)(I + G_oF)^{-1}\right\|_\infty < 1$" has been satisfied for the nominal system. In Fig. 7 the closed-loop system singular values for a frequency range of $[10^{-2} \quad 10^5]$ rad/sec are shown. It can be confirmed from the figure that the maximum magnitude is about 0.145 and is maintained constant over a frequency range of about 0.1 rad/sec to 100 rad/sec.

In Fig. 8, the magnitude of $1/\alpha(s)_p$ and that of the *sensitivity function* are compared. It is observed that, over the entire frequency range, magnitudes of the *sensitivity function* lie below those of the inverse of *performance weighting function*. The implication is that, over the entire simulation frequency range, it is guaranteed that singular values of the sensitivity function lie below those of $1/\alpha(s)_p$.

For *structured* uncertainty, *robust stability* and *performance* investigations require the frequency response in terms of *structured singular values* (SSV) [19] (also called the μ-value). Our concern is to obtain the upper and lower bounds for μ-values. The MRCT command mu can be used for this purpose. For the steps involved in μ-analysis [19]:

1. Recast the problem into the standard "$M - \Delta$" structure of Fig. 9, where the transfer function matrix $M$ denotes the lower LFT of the open-loop system w.r.t the controller $F$. Δ denotes the uncertainty matrix.
2. Compute the frequency response of $M$. It can be proved that the system in Fig. 9 achieves robust stability over all Δ if and only if the maximum SSV value over all frequencies is less than unity according to:

$$\mu\_\Delta=[M(j\omega)]<1 \tag{24}$$

3. Define the structure of the perturbation matrix Δ.
4. Compute the SSV bounds w.r.t the defined uncertainty. The MRCT command mu can be utilized.

For *robust stability*, it is required that the upper bound of SSV should be less than 1 over the entire frequency range. In *robust stability* investigation, our concern is investigating how robust the model is to *uncertainty*.

The computation results obtained are given in table III. The peak (i.e. upper bound) of $\mu_\Delta = [M(j\omega)]$ is obtained as 0.6160 and its lower bound is obtained as 0.4068. The interpretation of this numerical value is that, for all *structured* perturbation matrices ($\Delta\epsilon\Delta$) satisfying:

$$\max_{\omega} = \bar{\sigma}[\Delta(j\omega)] < \frac{1}{0.616}$$

the system will remain *robustly stable* at all frequency. This can also be confirmed from Fig. 10 where the responses for the upper and lower bounds of SSV are plotted. For the purpose of comparison, we also plot the singular values of *M*. Over all frequencies, SSV values are less than 1 and hence *robust stability* is guaranteed.

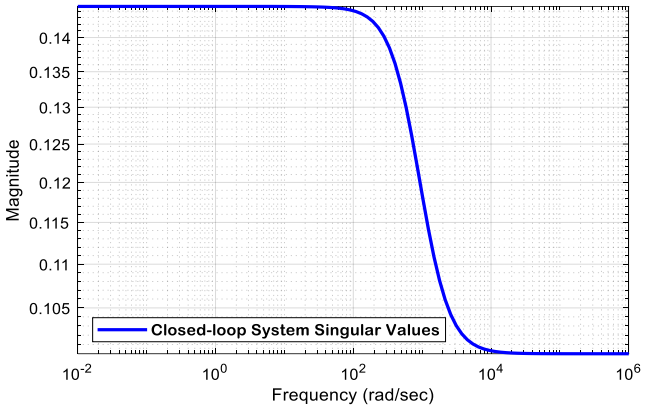


**Figure 7: Closed-loop system singular values plot**

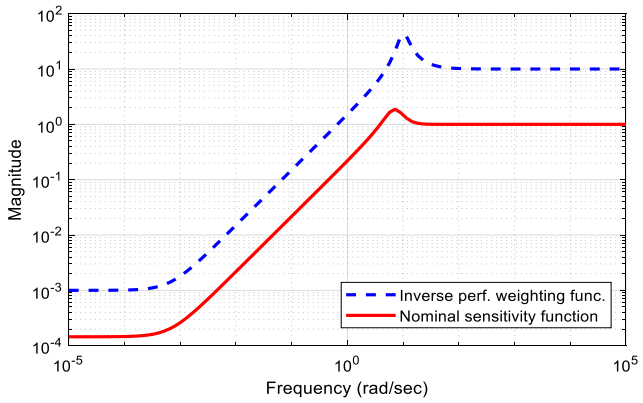


**Figure 8: Inverse performance weighting function and sensitivity function comparison**

According to what is commonly known as (Doyle 1982) [20], another benefit of $\mathcal{H}_\infty$ norm for *performance* as well as for *uncertainty* is the fact that *robust stability problem* may be recast as a *robust performance problem*. The robust performance requirement can be incorporated into the uncertainty matrix as a "fake uncertainty block". By doing so, the condition in (24) can be extended to incorporate this modification and can be re-written as:

$$\mu_{\tilde{\Delta}} = [T(j\omega)] < 1, \qquad \forall\omega \tag{25}$$

where $T$ represents the transfer function from the exogenous disturbance $d$ to the performance error $e$ and $\tilde{\Delta}= diag(\Delta, \Delta_P)$. $\Delta_P$ is the "fake uncertainty block" to allow for *performance* requirement.

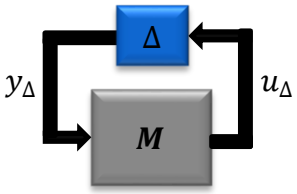


**Figure 9: LFT configuration for robust stability analysis**

**Table III: Structured singular values for robust stability**

| μ-bound | Value | Frequency | μ-Margin |
|---|---|---|---|
| **Upper:** | 0.6160 | 9.77 rad/sec | 0.2092 |
| **Lower:** | 0.4068 | 25.5 rad/sec | |

For *robust performance*, the steps involved in μ-analysis are similar to those presented for *robust stability*, except that the system is configured in the form shown in Fig. 11 which incorporates the exogenous disturbance $d$ and the performance error $e$ that characterizes the performance objective. Likewise, like in the case of *robust stability*, for *robust performance* it is a requirement that SSV upper-bound should <1 over the entire frequency range. But, in *robust performance* study, our concern is investigating how robust the model is to disturbance. The computation results obtained for *robust performance* are given in table IV. The peak (i.e. upper bound) of $\mu_{\tilde{\Delta}} = [M(j\omega)]$ is obtained as 0.7106 and its lower bound is obtained as 0.6980. The engineering meaning of these numerical values is that, for all *structured* perturbation matrices ($\Delta\epsilon\tilde{\Delta}$) satisfying:

$$\underset{\omega}{max} = \bar{\sigma}[\Delta(j\omega)] < \frac{1}{0.7106}$$

the system maintains *robust performance*. This can also be confirmed from Fig. 12, where the *nominal* and *robust performances* of the system with $\mathcal{H}_\infty$ were studied. For comparison purpose, the SSV values of $M$ are also plotted. Over all frequencies, SSV values are less than 1 and hence *nominal* as well as *robust performance* are guaranteed. These deductions are based on the fact that the frequency responses of the *nominal performance* and *robust performance* all have magnitudes less than 1 at all frequencies over the frequency range $0.1 - 100$ rads/sec. It may have been observed that the effect of the disturbance resulted in narrowing of the $\mu - margin$ by about 94%.

**Table IV: Structured singular values for robust performance**

| μ Bound | Value | Frequency | μ-Margin |
|---|---|---|---|
| **Upper:** | 0.7106 | 0.87 rad/sec | 0.0126 |
| **Lower:** | 0.6980 | 0.81 rad/sec | |

We investigated the system's *robustness* with the designed controller based on frequency response. We will proceed to study the robustness of the system based on time-response criteria. The goal is a maximum overshoot of 25%, and the system is required to reach steady state in less than 10 seconds. In Fig. 13, the transient response of the full-order and the reduced-order controller to step change in command were studied. It can be seen that there were no significant differences in performance. Yet, it is worth to note that the reduced-order controller was relatively slower than the full-order controller. As given in Table V, maximum overshoots of about 22% were observed and settling times were less than 10 seconds for all controllers. Also, in Fig. 14, the transient responses to unity magnitude disturbance outputs of the two controllers were studied. Disturbance signals with durations of 10 seconds were injected at 15 and 45 seconds. It was observed that the full-order and reduced-order controllers were robust to the output disturbance with maximum overshoots of about 21% and 22.4% respectively. Also, settling times for full and reduced-order controller were about 3 seconds and 9 seconds with respect to order. We have seen in Table II that the 4th and 5th states contribute less to the dynamics of the full-order controller, thus, we obtained a 3rd-order controller. Based on *Hankel norm* values, a 2nd-order controller cannot meet *robustness* requirements. This claim has been examined in Fig. 15 where oscillatory transient responses were observed.

**Table V: Transient responses to step tracking and disturbance**

| | Response to Step | | Response to Dist. | |
|---|---|---|---|---|
| **Controller Order** | **OS (%)** | **Settling Time(s)** | **OS (%)** | **Settling Time(s)** |
| **5th** | **21** | **3** | **21** | **3** |
| **3rd** | **22.4** | **8** | **22.4** | **9** |

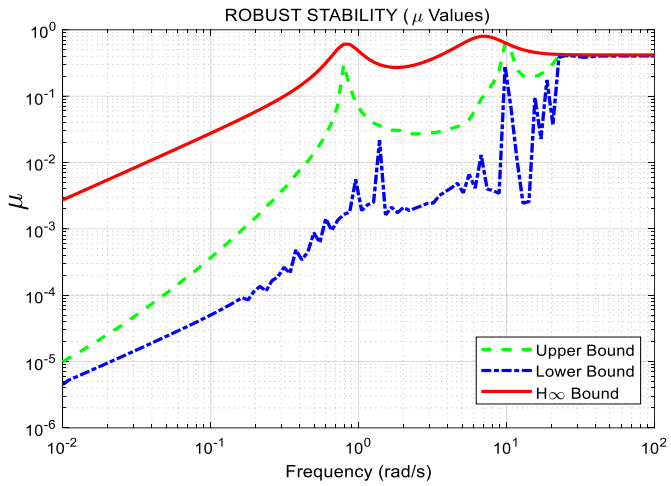


**Figure: 10 SSV bounds for robust stability studies**

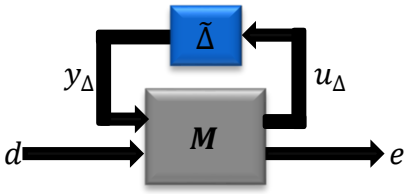


**Figure 11: LFT configuration for robust performance analysis**

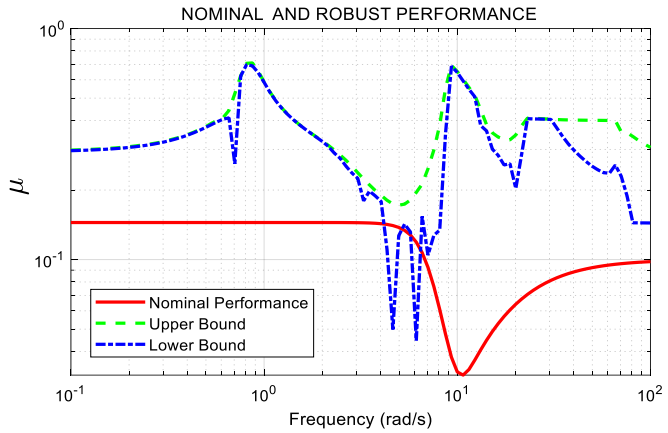


**Figure 12: SSV bounds for nominal and robust performance studies**


**Figure 13: Transient response to reference command tracking with $\mathcal{H}_\infty$ controller**

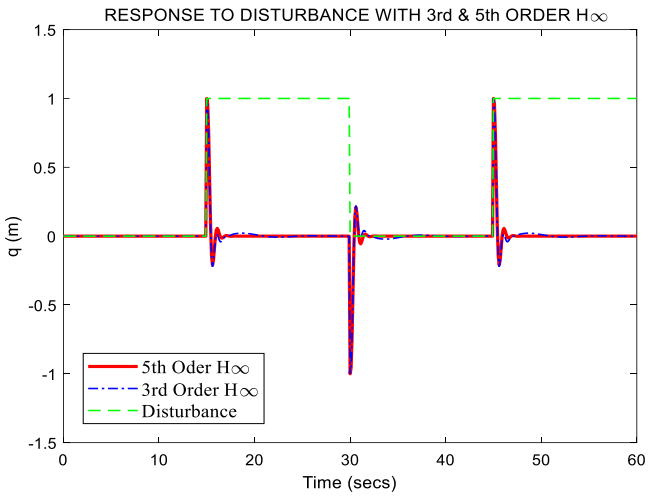


**Figure 14: Transient response to disturbance with $\mathcal{H}_\infty$ controller**

## Conclusion and Recommendations

In this work, the discrepancies between the practical mass-spring-dashpot system and the nominal system were evaluated and uncertainty modelling was conducted. A third-order controller was synthesized where a $\mathcal{H}_\infty$ norm of 0.145 was achieved. It was shown using μ-analysis that using the designed controller the system was able to achieve both robust stability and performance in the presence of uncertainties and disturbance. The effect of a unit disturbance on the set-point tracking error at steady-state was minimal. Also, transient response results showed that the control system achieved the specified requirement of overshoot and settling time. An overshoot of 22.4% and a settling time of 9 seconds were recorded as worst-case performance. We conclude that the objectives of the study have been achieved. In design, there may be some noticeable discrepancies in performances between the synthesized full order controller and the reduced order controller. Also, in practical scenario, there may be discrepancy in accuracy between the designed controller and the implemented controller. These cases are crucial and can be included as uncertainty during design to allow for better accuracies in design and implementation.

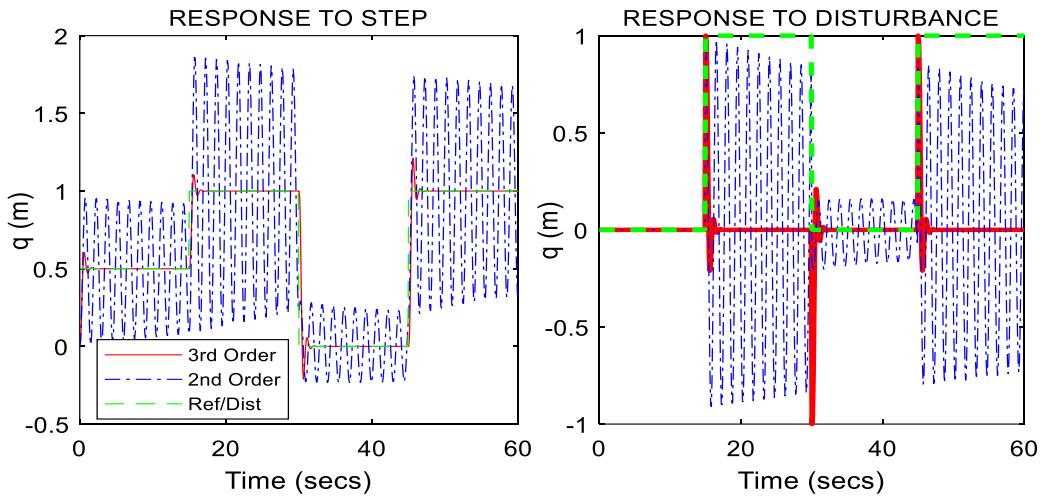


**Figure 15: Transient response to reference command tracking with second order $\mathcal{H}_\infty$ controller**

# REFERENCES

1. T. Badings, et al., "Robust Control for Dynamical Systems with non-gausian Noise via Formal Abstraction," Journal of Artificial Intelligence Research, vol. 76, pp. 341-391, 2023.
2. K. J. Åström, R. M. Murray, Feedback Systems: An Introduction for Scientists and Engineers, 41 William Street, Princeton, New Jersey: Princeton University Press, 2008.
3. P. Petkov, J. Kralev, "Design and Implementation of Robust Control Laws," in 29th European Conference on Modelling and Simulation, Sofia, 2015, pp. 6-18.

4. X. Tong, et al., "Model-free Adaptive Dynamic Event-triggered Robust Control for Unknown Nonlinear Systems using Iterative Neural Dynamic Programming," Information Sciences, vol. 655, 119866, 2024.
5. S. Skogestad, I. Postlethwaite, Multivariable feedback control: analysis and design, 2nd ed. John Wiley & Sons, 2001.
6. D. Barros, S. Fekri, M. Athans, "Robust mixed-μ synthesis performance for mass-spring system with stiffness uncertainty," in Proc. the 20th IEEE International Symposium on Intelligent Control, ISIC '05 and the 13th Mediterranean Conference on Control and Automation, MED '05, 2005, pp. 743–748.
7. W. Reinelt, "Robust Control of a Two-Mass-Spring System Subject to its Input Constraints," Proceedings of the 2000 American Control Conference, Chicago, IL, June 2000, pp. 1817-1821 vol.3.
8. Y. S. Kim, "Robust Control Design and Analysis Using SCILAB," Appl. Mech. Mater., vol. 300–301, no. 1, pp. 1423–1429, 2013.
9. C. I. Marrison, R. F. Stengel, "Robust Control System Design Using Random Search and Genetic Algorithms," IEEE Transactions on Automatic Control, vol. 42, no. 6, pp. 835–839, 1997.
10. A. Farag, H. Werner, "Robust $H_2$ Controller Design and Tuning for the ACC Benchmark Problem and a Real-Time Application," 15th Triennial World Congress, Barclona, Spain, 2002, pp. 2–7.
11. D. Wang, C. Mu, "Adaptive-Critic-Based Robust Trajectory Tracking of Uncertain Dynamics and Its Application to a Spring–Mass–Damper System," in IEEE Transactions on Industrial Electronics, vol. 65, no. 1, pp. 654-663, Jan. 2018.
12. C. W. De Silva, Frontmatter Vibration Fundamentals and Practice, Boca Raton: CRC Press, 2000.
13. S. S. Rao, Mechanical Vibrations, 5th ed. 1 Lake Street, Upper Saddle River, NJ: Prentice Hall, 2011.
14. D. J. Inman, Engineering Vibrations, 4th ed. Upper Saddle River, NJ: Pearson Education, 2014.
15. G. Takács, B. Rohal'-Ilkiv, Model Predictive Vibration Control, London: Springer, 2012.
16. R. Y, Chiang, M. G, Safonov, The MATLAB Robust Control Toolbox, Version 2, Cochituate Place, 24 Prime Park Way, Natick, Mass, 01760: The MathWorks, Inc., 2000.
17. J. Hu, C. Bohn, H. R. Wu, "Systematic H∞ weighting function selection and its application to the real-time control of a vertical take-off aircraft," Control Eng. Pract., vol. 8, no. 3, pp. 241–252, 2000.
18. B. Chaudhuri, B. C. Pal, A. C. Zolotas, I. M. Jaimoukha, T. C. Green, "Mixed-Sensitivity Approach to H∞ Control of Power System Oscillations Employing Multiple FACTS Devices," IEEE Transactions on Power Systems, vol. 18, no. 3, pp. 1149–1156, 2003.
19. R. Y, Chiang, M. G, Safonov, μ-Synthesis Toolbox User's Guide For Use with MATLAB, Version 3, 3 Apple Hill Drive Natick, MA 01760-2098: The MathWorks, Inc., 2001.
20. J. Doyle, "Analysis of feedback systems with structured uncertainties," in IEE Proceedings D - Control Theory and Applications, vol. 129, no. 6, pp. 242-250, November 1982.
21. U. Zulfiqar, M. Imran, A. Ghafoor, "Cross-Gramian based frequency-weighted model order reduction technique," in Electronics Letters, vol. 52, no. 16, pp. 1376-1377, 8 4 2016.



**CITATION**
M.A.Baballe, M.A.Shehu, A.A.Umar, A. Surajo, & H.G.Rabo. (2024). Application of Reduced-order Suboptimal H_∞ Control for Vertical Oscillation Damping in Mass-spring-dashpot Systems. In Global Journal of Research in Engineering & Computer Sciences (Vol. 4, Number 1, pp. 46–58). https://doi.org/10.5281/zenodo.10651888